Journal of Materials Chemistry C

ROYAL SOCIETY OF CHEMISTRY

COMMUNICATION

View Article Online
View Journal | View Issue

Cite this: J. Mater. Chem. C, 2024, 12, 15888

Received 23rd June 2024,
Accepted 1st August 2024

DOI: 10.1039/d4tc02624a

rsc.li/materials-c

Multiple-resonant nitrogen embedded nanographenes with high photoluminescence efficiency and high colour purity†

Hao Luo,‡[ab] Jinbei Wei,‡[a] Minqiang Mai,‡[c] Xuan Zeng,[c] Weifeng Zhang,[a] Xuyang Wei,[ab] Dongdong Zhang,*[c] Lian Duan[c] and Gui Yu *[ab]

A feasible approach by decorating π-extensions with nitrogen is proposed to realize narrow-band emitting NGs with multiple resonance (MR) effect. Pure blue and green NGs were obtained under mild reaction conditions in high yields. Both NGs featured high photoluminescence quantum yields (>90%) with emission peaks at 454 and 516 nm, small full widths at half maxima (FWHMs) of 18 and 23 nm, and high colour saturation with *y*-coordinates of 0.083 and 0.73, respectively. OLEDs using these NGs as emitters exhibited ideal blue (459 nm) and green (532 nm) emissions with high colour purity and small FWHMs of 25 and 21 nm, respectively.

Nanographenes (NGs), a group of fractured segments of graphene, have attracted considerable research interest due to their intriguing optical, electronic, magnetic and spintronic properties.[1–3] The vast family of NGs consists of miscellaneous molecules with unique topological features and accessible structural modifications through chemical reactions, fostering research in the preparation and application of NGs in organic electronics. Over the past two decades, preparation techniques for NGs have been extensively studied, typified by substrate-assisted on-surface synthesis and solution-phase synthesis.[4–7] In particular, NGs obtained by solution-based chemical reactions are structurally well-defined and transferable to device processing, becoming the primary approach for the applications of NGs.[8,9] In this way, all-carbon NGs were first synthesized and their properties were reviewed. Although covered by a large family, including corannulene (COR), hexabenzocoronene (HBC) and their derivatives (Fig. 1a), the poor properties of low photoluminescence quantum yields (PLQYs), multiple emission peaks and inert chemical reactivities deny any possible applications using all-carbon NGs.[10–12] To date, the applications of all-carbon NGs remain scarce and limited in organic field effect transistors (OFETs) with low carrier mobilities due to poor processability from low solubility.[13,14] To manipulate the optoelectronic properties of NGs, the insertion of heteroatoms, especially nitrogen, has proved to be a robust tactic as it can disrupt the all-carbon skeleton.[15–17] The electronic structure of N-doped NGs can be well modified by doping mode (position, co-doping and amount), thus being able to achieve superior physical properties including reactivity, photophysical features, carrier mobility and self-assembly in solution through rational molecule design and viable synthetic routes.[9,18,19] Recently, NGs containing nitrogen heterocycles have been widely used as charge transport channels in OFETs, showing excellent charge transport capabilities. For example, Liu's group fused carbazole and dibenzothiophene units into NG ribbons, which gave an excellent hole mobility of over 2.0 $cm^2 V^{-1} s^{-1}$ in OFET devices.[20,21] In addition, Ito *et al.* also proposed a pyrrole-fusing thiepine nanographene, and a high hole mobility of 1.0 $cm^2 V^{-1} s^{-1}$ was recorded in OFET measurement.[22]

Despite the good performance as transport materials, most of these NGs perform poorly as emitters due to their broad emission spectra with multiple peaks caused by vibronic coupling between the ground state (S_0) and singlet excited state (S_1) as well as structural relaxation at the S_1, resulting in poor colour purity and therefore not suitable for luminescent devices.[23] In addition, the strongly close packing mode in the solid state will inevitably cause severe aggregation-caused quenching. In pursuit of highly monochronic luminescent NGs, one viable tactic is to insert nitrogen atoms in the body of NGs in order to separate the distribution of the highest occupied molecular orbital (HOMO) and the lowest unoccupied

[a] Beijing National Laboratory for Molecular Sciences, CAS Research/Education Center for Excellence in Molecular Sciences Institute of Chemistry, Chinese Academy of Sciences, Beijing 100190, China. E-mail: yugui@iccas.ac.cn
[b] School of Chemical Sciences, University of Chinese Academy of Sciences, Beijing 100049, China
[c] Key Lab of Organic Optoelectronics and Molecular Engineering of Ministry of Education Department of Chemistry, Tsinghua University, Beijing 100084, China. E-mail: ddzhang@mail.tsinghua.edu.cn

† Electronic supplementary information (ESI) available. CCDC 2240856. For ESI and crystallographic data in CIF or other electronic format see DOI: https://doi.org/10.1039/d4tc02624a

‡ All marked authors contributed equally to this work.

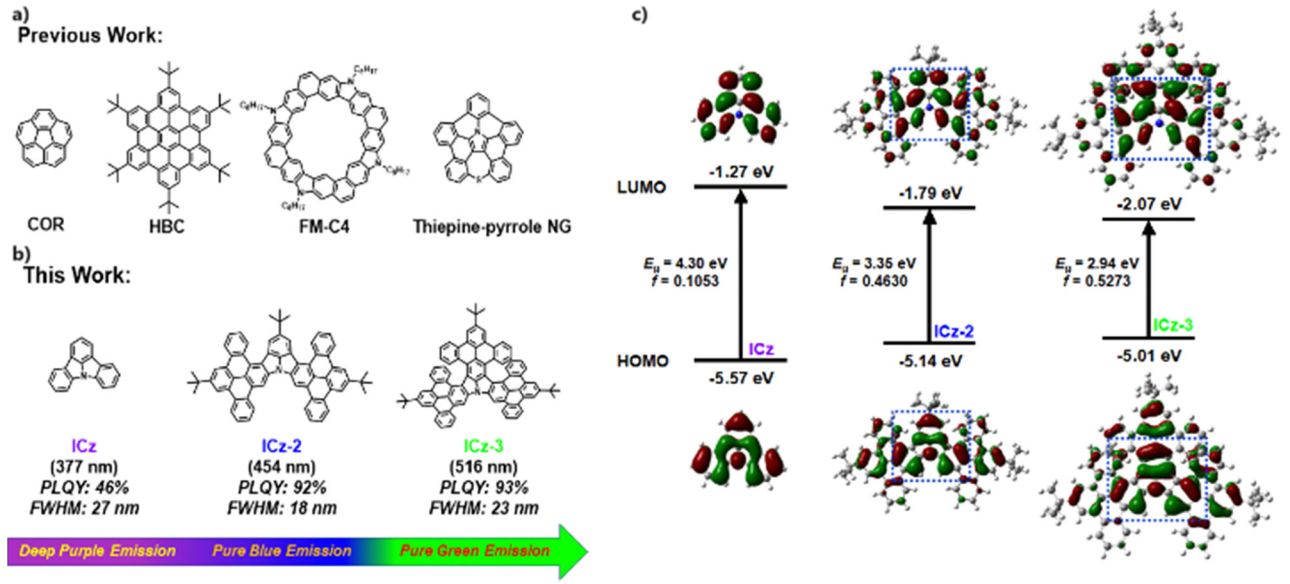

Fig. 1 (a) The molecule structures of some typical all-carbon NGs and N-embedded NGs. (b) The molecule structures and molecular design strategy of novel N-doped NGs. (c) The HOMO/LUMO distributions of ICz, ICz-2 and ICz-3 calculated by TD-DFT.

molecular orbital (LUMO) at the single atom scale, which is considered as multiple resonance (MR). As a result, narrow-band emissions have been obtained in synergy with introducing donors/acceptors or stretching π conjugations.[24–26] Despite this, the synthesis towards these MR-type materials has inevitably suffered from long, sophisticated synthetic routes and low yields from key steps, not to mention several notoriously hazardous operations. Alternatively, the search for functionalized N-embedded NGs with narrow-band emission should be intriguing but challenging. Regarding this, indolo[3,2,1-*jk*]carbazole (ICz) could be a proper model to undertake extensive research into. ICz serves as an ideal prototype due to its excellent properties with MR effects throughout the molecule.[27] In addition, the deep purple emission at 377 nm, the ultra-small photoluminescence (PL) full width at half maximum (FWHM) of 27 nm, and a large energy gap (E_g) of 4.30 eV allow much room for performance improvement and structure decoration of ICz in terms of modifying the photophysical properties. In addition, high chemical reactivity is present at three *para*-N sites, permitting such developments to be achieved through chemical reactions.

In this context, we conceive a new group of ICz-NGs by stretching along the axes of *para*-N positions and attaching different numbers of π-segments at the periphery, as shown in Fig. 1b. By simple and effective Suzuki coupling and Scholl oxidative cyclization,[28–30] the ICz core was decorated with two/three dibenzo[*e*,*l*]pyrene (DBP) wings, yielding ICz-2 and ICz-3 with high total yields without any risky operations. The direct fusions at the periphery allowed proper red-shifted emissions at 454 and 516 nm, respectively, together with maintaining the narrow-band character of ICz (FWHMs of 18 and 23 nm) and obtaining high PLQYs (92% and 93%) and CIE_y of 0.083 and 0.73, respectively. The excellence of high colour purity and effective luminescence resulted in superior electroluminescent (EL) performance in devices using ICz-2 and ICz-3 as emitters, with EL peaks at 459 nm and 532 nm, FWHMs of 25 and 21 nm, and moderate maximum external quantum efficiencies (EQE_{max}) of 3.8% and 12.5%, respectively.

To estimate the effect of π-extensions of DBP on the electronic and optical properties of ICz-NGs, time-dependent density functional theory (TD-DFT) using B3LYP-D3/6-31G(d,p) was carried out. The HOMO/LUMO distributions of ICz, ICz-2 and ICz-3 with their corresponding oscillator strengths (*f*) are displayed in Fig. 1c. As a typical MR-type compound, the HOMO/LUMO in ICz adopted alternate distributions centered by an N atom. It was expected that the MR effect was well reserved in ICz-2 and ICz-3 after fusing with additional π-segments at the periphery of ICz. Moreover, the delocalized orbitals were aligned over the whole molecule, implying that effective conjugation happened in both ICz-NGs. As a result, the π-extended ICz-NGs exhibited smaller E_gs with 3.35 and 2.94 eV for ICz-2 and ICz-3, respectively, in contrast with that of 4.30 eV of ICz. The concept of π-extensions to reduce the E_g, unlike introducing charge-transfer, undercut possible broadened emission character, as the HOMO/LUMO were evenly distributed over the ICz-NGs. As a result, smaller reorganization energy of less than 0.20 eV was obtained in both ICz-NGs, which is in favor of high colour purity emissions due to suppressed vibronic couplings and structural relaxations (Fig. S1, ESI†). Furthermore, the stretched delocalization of molecular orbitals in ICz-2 and ICz-3 favored larger *f* values of 0.4630 and 0.5273, respectively, indicating the fast radiation decay process. The enlarged π-conjugation systems guaranteed properly reduced E_gs and intensified *f* by the virtue of the MR-type HOMO/LUMO distribution, which in turn granted ICz-NGs with narrow-band emissions and high radiant decay rates (k_rs).

As described in Scheme 1 and Scheme S1 (ESI†), both ICz-2 and ICz-3 were synthesized through Suzuki–Miyaura coupling and Scholl oxidative cyclization. Generally, the *tert*-butyl substituted

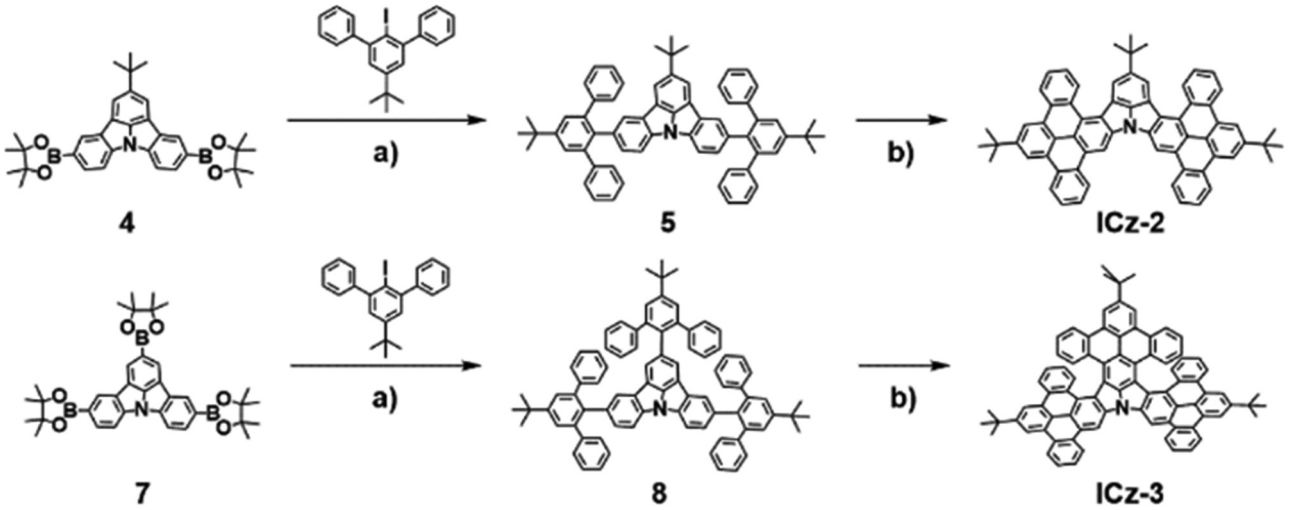

Scheme 1 Synthesis of ICz-2 and ICz-3. Reagents and conditions: (a) K_2CO_3, $Pd(PPh_3)_4$, H_2O/1,4-dioxane, reflux for overnight; (b) $FeCl_3$, CH_3NO_2/CH_2Cl_2, 0 °C for 30 min.

triphenylbenzene moiety was introduced into the ICz skeleton and then the cyclization process took place with the existence of $FeCl_3$. The synthesis procedure is free of dangerous alkyl lithium reagents with low yields. However, the borylated compounds **4** and **7** were obtained differently. For compound **7**, a string of high-yield reactions, including C–H activation of *N*-phenyl carbazole forming ICz, triple bromination of ICz and subsequent Miyaura borylation by bis(pinacolato)diboron, were implemented. Meanwhile, compound **4** was synthesized in a similar pattern except that the pre-occupied *tert*-butyl group (–*t*Bu) at one site of the *para*-N position was introduced in an otherwise way. The *t*Bu-substituted ICz (**2**) was synthesized by palladium^0-catalysed Buchwald–Hartwig coupling, followed by bromination using NBS and Miyaura borylation. ICz-2 and ICz-3 were obtained as yellow and orange powders with yields of 76% and 68%, respectively. The newly synthesized NGs, alongside the intermediates, were clearly

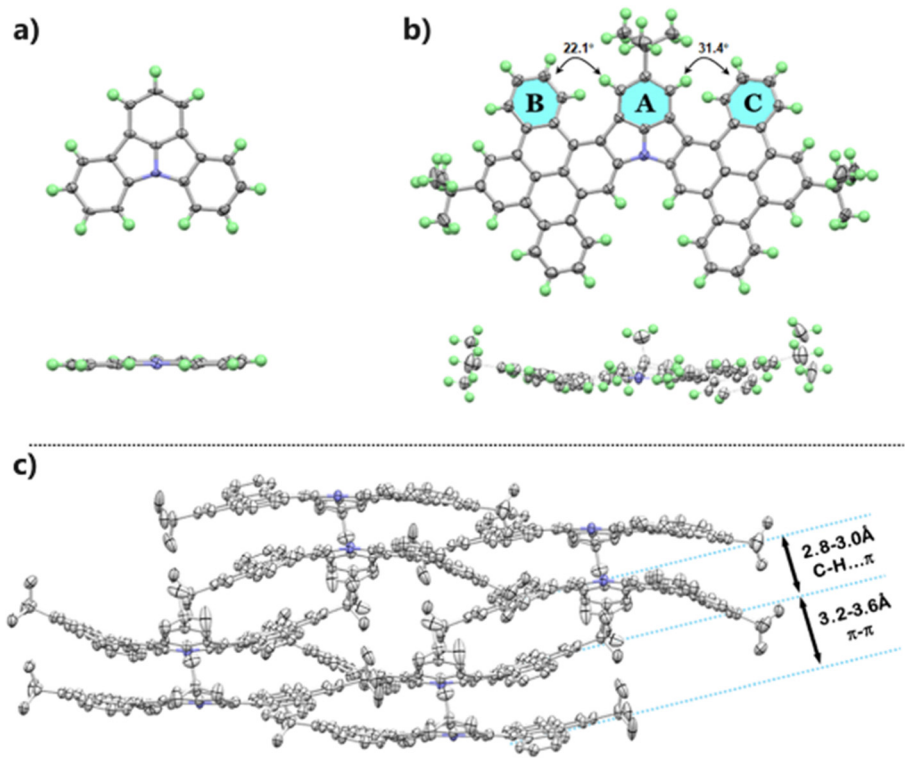

Fig. 2 ORTEP drawings of (a) ICz and (b) ICz-2 obtained by single crystal X-ray diffraction at the 50% possibility level. Top-view (top) and side-view (bottom) are shown. (c) Packing structure of ICz-2. Solvent molecules (toluene) and hydrogen atoms in the crystal structure of ICz-2 are omitted for clarity.

characterized by ^{1}H NMR spectra and high-resolution mass spectra (Fig. S2–S19, ESI†). Both NGs demonstrated good thermal stability with decomposition temperatures (5% weight loss) over 490 °C, as explored by thermal gravimetric analysis (Fig. S20, ESI†), which is the intrinsic requirement for OLED fabrication.

The single crystal of ICz-2 suitable for X-ray analysis was obtained by slow diffusion of methanol into a toluene solution of ICz-2. Compared to the parent core with a quite planar structure (Fig. 2a), ICz-2 is a slightly twisted molecule with two symmetrical DBP wings on the ICz core, as the molecule drawings from top view and side view drawn in Fig. 2b. The dihedral angles between the ICz core (represented by ring A) and DBP segments (ring B and C) were 22.1° and 31.4°, while the inner ICz core remained as planar as the original ICz molecule. The torsion existed because of the repulsion of adjacent hydrogen atoms from ring A and ring B/C. After Scholl oxidative coupling, the newly formed DBP segment lacked free rotation and deviated from the central plane to avoid such repulsion. The uneven dihedral angles, to some extent, were attributed to the special packing pattern of ICz-2 crystal. Depicted in Fig. 2c, one pair of ICz-2 molecules adopted distinctively π–π stacking by overlapping aromatic rings in a bowl-piling type, with moderate distances from 3.2–3.6 Å. The shallow bowl-like molecule pairs were aligned in the *xy*-plane and packed in a back-to-back pattern along the *z*-axis in the unit cells. The closely stacked planes, where the interlayer distances were approximately 2.6–3.0 Å, were linked by intermolecular C–H···π hydrogen bonding. Given the strong stacking behaviors, the emissions of ICz-NGs in the powder states were negatively influenced with broadening and low PLQYs less than 4% (Fig. S22, ESI†).

We further investigate the photophysical properties of ICz-2 and ICz-3 in 10^{-5} M toluene solutions. Compared with ICz, which featured a strong absorption at 375 nm, the ICz-2 and ICz-3 showed maximum absorptions at long wavelengths with 445 nm and 511 nm, respectively, shown in Fig. 3a. In the fluorescence spectra (Fig. 3b), redshifted emission peaks were found at 454 nm for ICz-2 and 516 nm for ICz-3. The emission spectra for both ICz-NGs are in good correlation with calculated spectra carried out by TD-DFT, as shown in Fig. 3c and d. Compared with the calculated emission spectrum of ICz depicted in Fig. S23 (ESI†), smaller FWHMs of 17 and 14 nm for ICz-2 and ICz-3, respectively, were predicted after the addition of π-extensions of the DBP units. The small Stokes shifts, both less than 10 nm, were significantly attributed to the MR-type ICz core and π-extensions of ICz-derived NGs. It is worth mentioning that the shoulder peaks in the emission spectra of both ICz-2 and ICz-3 cannot be ignored. The splits in the peaks were ascribed to the incorporation of DBP blades at the periphery, and the combination of single-peak ICz and multiple-peak DBP gave rise to suppressed shoulder peaks in ICz-2 and ICz-3 (Fig. S24, ESI†). To our delight, both ICz-NGs

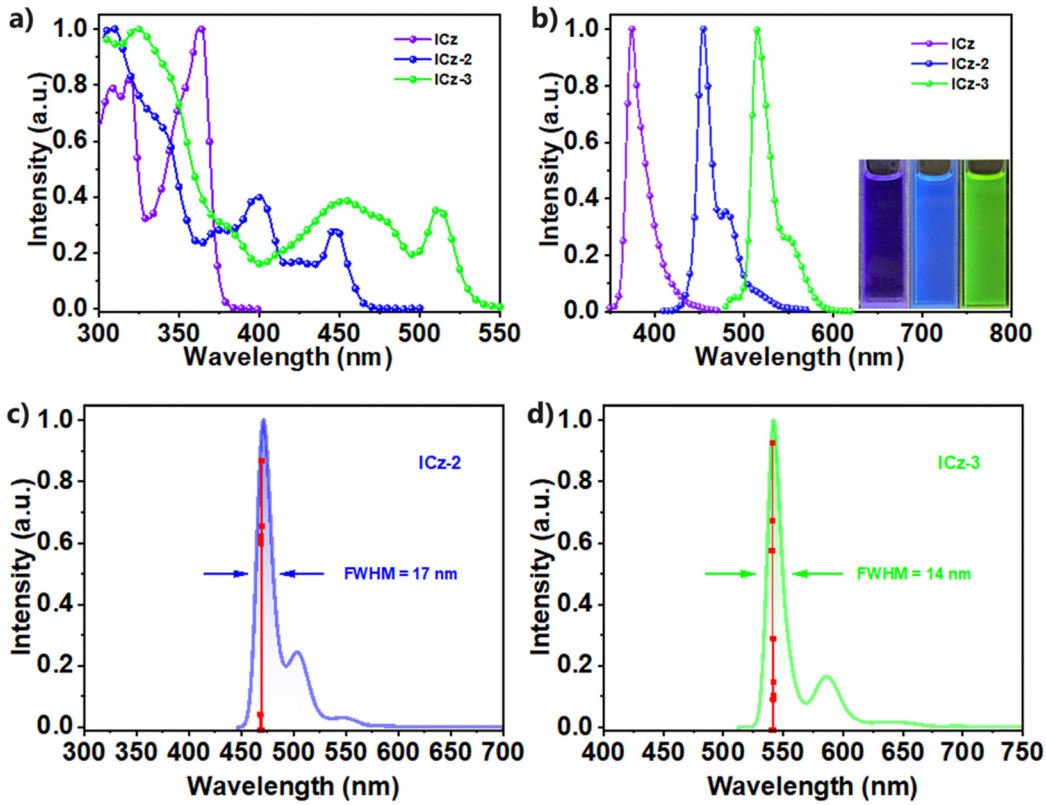

Fig. 3 (a) The absorption and (b) emission spectra of ICz, ICz-2 and ICz-3 measured in 10−5 M toluene solutions at 298 K. (c) and (d) Emission spectra of (c) ICz-2 and (d) ICz-3 simulated by Franck–Condon analysis (B3LYP-D3/6-31G(d,p)) on the S_1–S_0 transition in toluene broadening with a half width at half-maximum of 300 cm^{-1}. Dipole strength of each transition is marked by red dots.

possessed even smaller FWHMs of 18 (ICz-2) and 23 nm (ICz-3) than that of 27 nm for ICz, accompanied by high colour saturation with CIE_y of 0.083 and 0.73 (Fig. S25, ESI†), respectively. Furthermore, the emission spectra measured in different polar solvents for each ICz-NG were almost identical, as plotted in Fig. S26 (ESI†), demonstrating that no clear charge transfer was observed. The phosphorescence spectra of ICz-2 and ICz-3 measured at 77 K (Fig. S27, ESI†) indicated their respective triplet energy levels at 2.19 and 1.99 eV. Large singlet–triplet energy gaps (ΔE_{ST}s) of 0.54 and 0.41 eV were therefore obtained for ICz-2 and ICz-3. Moreover, the PL decay curves (Fig. S28, ESI†) showed single exponential features with lifetimes of 5.8 and 4.7 ns for ICz-2 and ICz-3, respectively. The large ΔE_{ST}s and prompt fluorescence lifetimes suggested that the ICz-NGs were conventional fluorophores with non-TADF characters. With photoluminescence quantum yields of 92% and 93%, both ICz-NGs displayed high k_rs of 1.6×10^8 s^{-1} for ICz-2 and 2.0×10^8 s^{-1} for ICz-3. The excellence in photophysical properties, summarized in Table 1, validated the rational design of ICz-NGs to manipulate redshifted emissions without trading out the intrinsic narrow-band feature of ICz.

To evaluate the potential application of ICz-NGs in EL devices, the photophysical properties of blend solid films were studied first. Owing to the non-TADF characters of both ICz-NGs, the compositions of the solid films followed the TADF sensitized fluorescence (TSF) system, which was constituted by the host material, TADF material, as a sensitizer and fluorophore. For the blue-light emitter, the films adopted PPF and CzBPCN as the host and TADF, respectively, while for the green-light emitter, mCBCP and 4TCzIPN were selected. PPF, CzBPCN, mCBCP and 4TCzIPN stand for bis(diphenylphosphoryl)dibenzo[*b*,*d*]furan, 4,4′,6,6′-tetra(9*H*-carbazol-9-yl)-[1,1′-biphenyl]-3,3′-dicarbonitrile, 9-(3-(9*H*-carbazol-9-yl)phenyl)-9*H*-3,9′-bicarbazole and 2,4,5,6-tetrakis-(3,6-di-*tert*-butyl-9*H*-carbazol-9-yl)isophthalonitrile, respectively, as shown in Fig. 4a. In the TSF films employing narrow-band emitters, selecting proper TADF materials is of significance to realize high colour purity in device applications. The matching emission characteristics of TADFs and fluorophores, plotted in Fig. S29 (ESI†), were validated by entirely overlapped emissions of ICz-NGs by that of corresponding TADF, which ensured the effective energy transfer between TADF and ICz-NGs. While for the selection of host materials, we consider the energy level to assist the injection of both holes and electrons, as well as high triplet energy level and high thermal stability. The emission spectra and PL decay curves of blue/green TSF films are depicted in Fig. S30 and S31 (ESI†), with gradient fluorophore doping concentrations up to 3.0 wt%. The emission spectra of the films were almost identical upon increasing fluorophore concentrations, whereas redshifted emissions were also observed in solid films due to π–π stacking. As the doping concentration increased, the FWHMs of both types of films employing ICz-2 and ICz-3 were slightly narrowed, further demonstrating the effective energy transfer from TADF to ICz-NGs. In the PL decay curves of the TSF films, TADF as sensitizers provided conspicuous delay component of the ternary compositions. On the contrary, the binary host/fluorophore films only exhibited prompt fluorescence similar to fluorophores, which again confirmed that ICz-NGs were conventional fluorophore. The EL spectra were measured with device structures schemed in Fig. 4b, where HATCN, NPB, TCTA, mCP, Bphen, and CzPhPy represent 1,4,5,8,9,11-hexaazatriphenylenehexacarbonitrile, 4,4′-bis[*N*-(1-naphthyl)-*N*-phenylamino]biphenyl, 4,4′,4′-tris(carbazol-9-yl)-triphenylamine, 1,3-bis(9*H*-carbazol-9-yl)benzene, 4,7-diphenyl-1,10-phenanthroline and 4,6-bis[3-(9*H*-carbazol-9-yl)phenyl] pyrimidine, respectively (Fig. S32, ESI†). The electroluminescent layers (EMLs) adopted ternary constitutions with 1.0 wt% fluorophore and 20 wt% TADF doped in the host material. For the blue OLED (device B), the device structure followed ITO/HATCN (5 nm)/NPB (30 nm)/TCTA (5 nm)/mCP (5 nm)/EML/PPF (10 nm)/Bphen (30 nm)/LiF/Al, while for the green OLED (device G), the device structure was ITO/HATCN (5 nm)/NPB (30 nm)/TCTA (10 nm)/EML/CzPhPy (10 nm)/Bphen (30 nm)/LiF/Al. Fig. 4c shows the EL spectra with peaks at 459 nm and 532 nm for device B and device G, respectively. Both devices exhibited super narrow narrow-band electroluminescence, with the FWHMs maintained at 25 and 21 nm, respectively. The narrow-band EL emissions remained the same with the dopant concentrations increased to 3.0 wt%, as illustrated in Fig. S33 (ESI†). Interestingly, we found that in diluted toluene solutions, the FWHMs of ICz-2 were smaller than that of ICz-3, while the EL FWHMs turned opposite as the device B owned a larger FWHM. One possible explanation was the strong π–π packing pattern of ICz-2. The bowl-like ICz-2 molecules were expected to be closely packed in solid films, accounting for fluorescence quenching by more intramolecular interactions and therefore broadening. In addition, the EL FWHM of device G employing ICz-3, 21 nm, was smaller than that in diluted toluene solution (23 nm). One possible explanation for this is owing to the participation of the sensitizer, 4TCzIPN. The matched photophysical properties are beneficial to the highly efficient process of energy transfer, which further introduces a further narrowed EL spectra. Accordingly, we further investigated the device performances employing ICz-2 and ICz-3. The external quantum efficiency–luminance (EQE–luminance) curves of the devices are plotted in Fig. 4d. A maximum EQE of 12.5% was observed in device G,

Table 1 Summary of the photophysical properties of ICz-2 and ICz-3

	λ_{Abs}[a] [nm]	λ_{em}[a] [nm]	λ_{phos}[b] [nm]	FWHM [nm]	S_1[a] [eV]	T_1[b] [eV]	ΔE_{ST} [eV]	HOMO[c] [eV]	LUMO[c] [eV]	E_g[d] [eV]	Φ_{PL}[e] [%]	τ[f] [ns]	k_r[g] [10^8 s^{-1}]
ICz-2	445	454	567	18	2.73	2.19	0.54	−5.71	−3.00	2.71	92	5.8	1.6
ICz-3	511	516	622	23	2.40	1.99	0.41	−5.57	−3.21	2.36	93	4.7	2.0

[a] Measured in 10^{-5} M toluene solution at 298 K. [b] Measured in 10^{-5} M toluene solution at 77 K. [c] Determined by circular voltammetry curves. [d] Determined by the onset of the absorption spectra. [e] Recorded as absolute quantum yield in diluted toluene solution with an integrating sphere system at 298 K. [f] Determined by photoluminescence decay curves in diluted toluene solution at 298 K. [g] Determined by this formula: $k_r = \Phi_{PL}/\tau$.

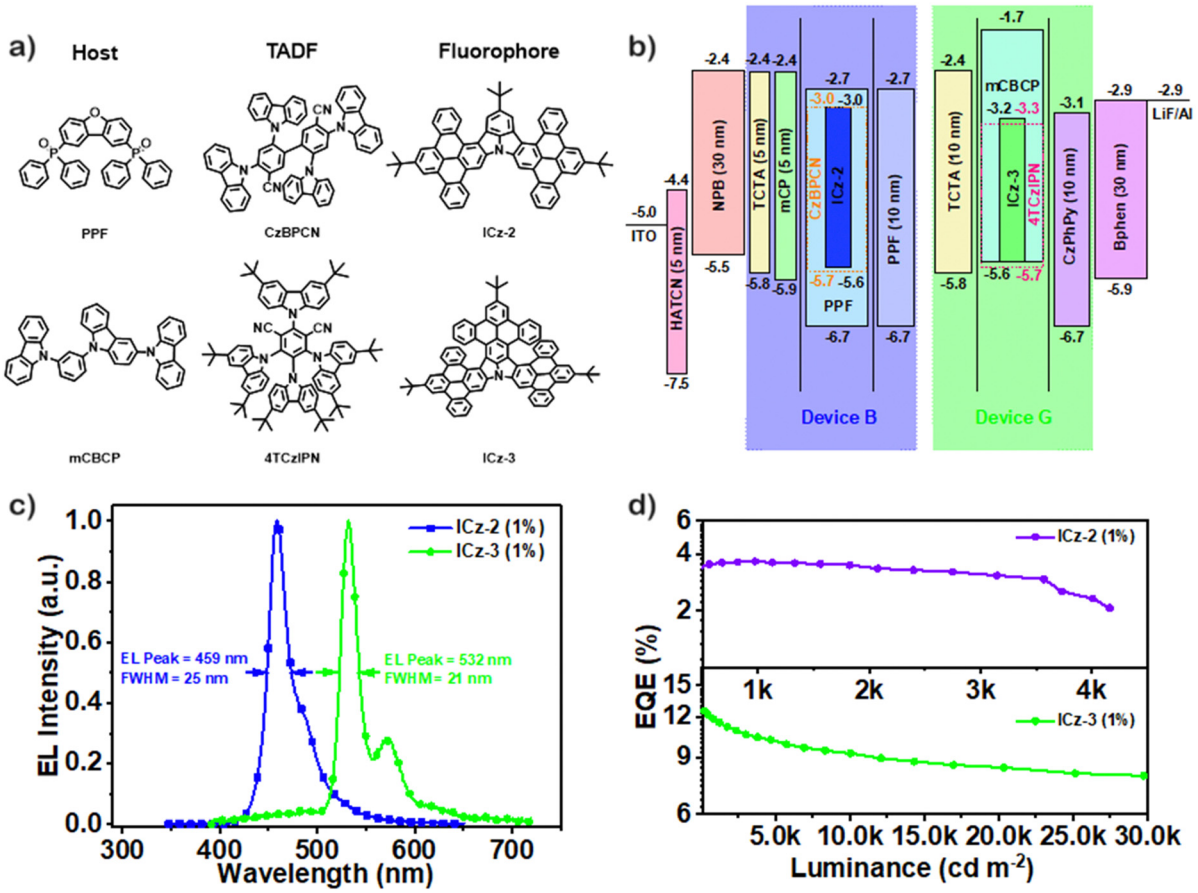

Fig. 4 (a) The molecule structures of materials used in the two TSF systems. (b) The energy levels of the devices. (c) The EL spectra of devices employing ICz-2 and ICz-3. (d) The EQE–luminance curves of the devices.

while that of the device B was only 3.8%. The underperformance of device B was presumably due to the low efficiency by CzBPCN as a sensitizer in the pure blue region and strong π–π packing of ICz-2.[31] Compared to the even lower EQEs based on similar ICz-based NG (3.3%), boosts in EL performance were observed in both devices employing ICz-NGs, benefitted from higher PLQYs.[27] Given this, the EL device for the ICz-NGs is left with much room for further exploration and development. To our best understanding, it is the first time that pure blue/green emitters are simultaneously constructed by N-doped NGs without introducing donors/acceptors or nonbonding orbitals in the molecule skeleton.

In conclusion, two ICz-NGs with π-extensions of DBP at *para*-N positions were successfully synthesized by Suzuki coupling and Scholl oxidative coupling with high yields. As conventional fluorophores, ICz-2 and ICz-3 exhibited excellent photophysical properties as blue and green emitters by the virtue of multiple resonance induced by the ICz core, with emission peaks in the pure blue/green region, narrow FWHMs and high PLQYs. Both ICz-NGs showed great potential in EL devices, with EL peaks at 459 and 532 nm, EL FWHMs of 25 and 21 nm, respectively, and moderate EQE_{max} of 12.5%. Our study provides a facile approach for manipulating the structure of ICz-derived N-embedded NGs with tuneable optical properties, sparking new insights for more NGs for promising organic electronic applications.

Author contributions

Gui Yu and Dongdong Zhang organized, guided and supervised the project. Hao Luo and Jinbei Wei proposed the idea and designed the experiments. Minqiang Mai fabricated the devices and tested the performances. Xuan Zeng, Xuyang Wei and Weifeng Zhang helped with the experiments and measurements. Hao Luo, Jinbei Wei and Minqiang Mai wrote and revised the manuscript. All authors have contributed to analyzing/curating data, drawing figures and preparing the manuscript. All authors have participated in discussing the results and reviewing the manuscript.

Data availability

The data supporting this article have been included as part of the ESI.† Crystallographic data for ICz-2 has been deposited at CCDC under 2240856† and can be obtained from **https://www.ccdc.cam.ac.uk**.

Conflicts of interest

There are no conflicts to declare.

Acknowledgements

The authors appreciate the financial support by the National Natural Science Foundation of China (22275194) and Beijing National Laboratory for Molecular Sciences (BNLMS-CXXM-202101).

Notes and references

1 S. Mishra, D. Beyer, R. Berger, J. Liu, O. Groning, J. I. Urgel, K. Mullen, P. Ruffieux, X. Feng and R. Fasel, *J. Am. Chem. Soc.*, 2020, **142**, 1147–1152.
2 I. Matsumoto, R. Sekiya, H. Fukui, R. D. Sun and T. Haino, *Angew. Chem., Int. Ed.*, 2022, **61**, e202200291.
3 P. J. Evans, J. Ouyang, L. Favereau, J. Crassous, I. Fernandez, J. Perles and N. Martin, *Angew. Chem., Int. Ed.*, 2018, **57**, 6774–6779.
4 J. Wang, C. Shen, G. Zhang, F. Gan, Y. Ding and H. Qiu, *Angew. Chem., Int. Ed.*, 2022, **61**, e202115979.
5 M. Daigle, A. Picard-Lafond, E. Soligo and J. F. Morin, *Angew. Chem., Int. Ed.*, 2016, **55**, 2042–2047.
6 M. Kolmer, R. Zuzak, A.-K. Steiner, L. Zajac, M. Engelund, S. Godlewski, M. Szymonski and K. Amsharov, *Science*, 2019, **363**, 57–60.
7 K. Xu, J. I. Urgel, K. Eimre, M. Di Giovannantonio, A. Keerthi, H. Komber, S. Wang, A. Narita, R. Berger, P. Ruffieux, C. A. Pignedoli, J. Liu, K. Mullen, R. Fasel and X. Feng, *J. Am. Chem. Soc.*, 2019, **141**, 7726–7730.
8 M. Stepien, E. Gonka, M. Zyla and N. Sprutta, *Chem. Rev.*, 2017, **117**, 3479–3716.
9 A. Borissov, Y. K. Maurya, L. Moshniaha, W. S. Wong, M. Zyla-Karwowska and M. Stepien, *Chem. Rev.*, 2022, **122**, 565–788.
10 J. Dey, A. Y. Will, R. A. Agbaria, P. W. Rabideau, A. H. Abdourazak, R. Sygula and I. M. Warner, *J. Fluoresc.*, 1997, **7**, 231–236.
11 P. Rietsch, J. Soyka, S. Brulls, J. Er, K. Hoffmann, J. Beerhues, B. Sarkar, U. Resch-Genger and S. Eigler, *Chem. Commun.*, 2019, **55**, 10515–10518.
12 K. Kato, Y. Segawa, L. T. Scott and K. Itami, *Angew. Chem., Int. Ed.*, 2018, **57**, 1337–1341.
13 Y. Sakamoto and T. Suzuki, *J. Am. Chem. Soc.*, 2013, **135**, 14074–14077.
14 S. H. Pun, Y. Wang, M. Chu, C. K. Chan, Y. Li, Z. Liu and Q. Miao, *J. Am. Chem. Soc.*, 2019, **141**, 9680–9686.
15 S. R. Peurifoy, T. J. Sisto, F. Ng, M. L. Steigerwald, R. Chen and C. Nuckolls, *Chem. Rev.*, 2019, **19**, 1050–1061.
16 E. Jin, Q. Yang, C. W. Ju, Q. Chen, K. Landfester, M. Bonn, K. Mullen, X. Liu and A. Narita, *J. Am. Chem. Soc.*, 2021, **143**, 10403–10412.
17 Y. Han, Z. Xue, G. Li, Y. Gu, Y. Ni, S. Dong and C. Chi, *Angew. Chem., Int. Ed.*, 2020, **59**, 9026–9031.
18 M. Zhao, S. H. Pun, Q. Gong and Q. Miao, *Angew. Chem., Int. Ed.*, 2021, **60**, 24124–24130.
19 W. Jiang, Y. Li and Z. Wang, *Acc. Chem. Res.*, 2014, **47**, 3135–3147.
20 N. Zhang, L. Yang, W. Li, J. Zhu, K. Chi, D. Chang, Y. Qiao, T. Wang, Y. Zhao, X. Lu and Y. Liu, *J. Am. Chem. Soc.*, 2022, **144**, 21521–21529.
21 N. Zhang, W. Li, J. Zhu, T. Wang, R. Zhang, K. Chi, Y. Liu, Y. Zhao and X. Lu, *Adv. Mater.*, 2023, **35**, e2300094.
22 W. Wang, F. Hanindita, Y. Tanaka, K. Ochiai, H. Sato, Y. Li, T. Yasuda and S. Ito, *Angew. Chem., Int. Ed.*, 2023, **62**, e202218176.
23 S. Madayanad Suresh, D. Hall, D. Beljonne, Y. Olivier and E. Zysman-Colman, *Adv. Funct. Mater.*, 2020, **30**, 1908677.
24 Y. Kondo, K. Yoshiura, S. Kitera, H. Nishi, S. Oda, H. Gotoh, Y. Sasada, M. Yanai and T. Hatakeyama, *Nat. Photonics*, 2019, **13**, 678–682.
25 X. Liang, Z. P. Yan, H. B. Han, Z. G. Wu, Y. X. Zheng, H. Meng, J. L. Zuo and W. Huang, *Angew. Chem., Int. Ed.*, 2018, **57**, 11316–11320.
26 X. F. Luo, S. Q. Song, H. X. Ni, H. Ma, D. Yang, D. Ma, Y. X. Zheng and J. L. Zuo, *Angew. Chem., Int. Ed.*, 2022, **61**, e202209984.
27 H. L. Lee, W. J. Chung and J. Y. Lee, *Small*, 2020, **16**, e1907569.
28 Y. Zhang, S. H. Pun and Q. Miao, *Chem. Rev.*, 2022, **122**, 14554–14593.
29 M. Grzybowski, K. Skonieczny, H. Butenschon and D. T. Gryko, *Angew. Chem., Int. Ed.*, 2013, **52**, 9900–9930.
30 M. Grzybowski, B. Sadowski, H. Butenschon and D. T. Gryko, *Angew. Chem., Int. Ed.*, 2020, **59**, 2998–3027.
31 Y. J. Cho, S. K. Jeon, S.-S. Lee, E. Yu and J. Y. Lee, *Chem. Mater.*, 2016, **28**, 5400–5405.

